PII: S0038-1098(98)00244-0

ON NANOTRIBOLOGICAL INTERACTIONS: HARD AND SOFT INTERFACIAL JUNCTIONS

Uzi Landman*

School of Physics, Georgia Institute of Technology, Atlanta, GA 30332-0430, U.S.A.

We address here certain aspects of the dependence of materials properties on their size, particularly at the nanometer length scale where new behavior emerges when the physical dimensions of the system approaches, or is reduced below, a characteristic length relevant for the phenomenon or physical process being probed. We focus on formation mechanisms, structural, mechanical, electronic, transport, dynamic and rheological properties of nanoscale hard (solid nanowires) and soft (confined liquid) interfacial junctions. These issues are central to research in nanotribology, that is exploration of the atomic and molecular scale origins of friction and lubrication and are relevant to modern minituarization technologies. © 1998 Elsevier Science Ltd. All rights reserved

Keywords: A. nanostructures, A. surfaces and interfaces, D. electronic transport, E. mechanical properties.

1. INTRODUCTION

That the properties of a material depend on the system's size is commonly expected and observed. Here we will inquire about circumstances where the reduction in system size is accompanied by the emergence of new phenomena and where the consequent physical properties cannot be deduced from those known for larger size systems (e.g. through simple scaling considerations). Such are the cases when inquiring about the room temperature conductance of a gold wire with a cross-sectional radius of the order of 10 Å (or a bismuth wire with a radius of several hundred Ångströms) and

whose length is smaller then the electron's mean free path, when asking about the force for sliding under certain normal loads an AFM (atomic force microscope) tip on a metal surface (i.e. does Amonton's law [13] apply?), or when attempting to estimate the shear stress required for sliding two solid interfaces with the lubricated gap between them (filled with a lubricant) reduced to widths of the order of 50 Å or less. In these cases, as well as in many other circumstances, fundamentally new physical behavior and response mechanisms appear when the physical size of the system becomes comparable to, or is reduced below, a characteristic length relevant for the phenomena underlying the physical processes being probed.

Such transition from a macroscopic to a "new behavior" regime, brought about by reduction in system size relative to some correlation, or other relevant, length scales, is also key to the emergence of mesoscopic phenomena [10, 11]. We remark however, that while certain aspects of the systems which we discuss share some common features with mesoscopic systems, the typical sizes that we address are much smaller, going down to the atomic and molecular scale. Furthermore, mesoscopics deals almost exclusively with phenomena of quantum mechanical origins and most often under special conditions (mostly low temperatures) while many of the nanoscale systems and the phenomena

---

* This paper was fashioned after my symposium lecture. As such it focuses on certain selected issues pertaining to nanotribology, illustrated mostly through my own experiences, rather than being a broad review and a comprehensive source for the large amount of published work in this area. Most of the work presented in this lecture was performed in collaboration with Robert N. Barnett, Jianping Gao and W. David Luedtke, with whom I co-authored the original papers and who should be considered also as co-authors of this one. If after reading the paper you wish to learn more about the subject, I have achieved my goal and you may consult the list of books and reviews cited at the end [1–12] as well as list of references.

discussed here are of classical nature and they occur at ambient (room temperature) environments.

By now the reader may have surmised that common to the aforementioned systems, brought above as examples, is their interfacial junction configuration; such is the case with a wire connecting two solids or stretching in the gap between a tip and surface, for a slider translated on a surface and in the case of a confined lubricating fluid filling the narrow gap between two opposing solid bodies set in shear motion with respect to each other. Understanding the formation mechanisms and physical (energetic, electronic, structural, mechanical, dynamic and rheological) properties of such solid (hard) and liquid (soft) interfacial junctions are principal subjects of modern research into the basic microscopic origins of tribological processes (tribology from the Greek word tribos meaning rubbing). Such processes, including friction, wear and lubrication occur in systems encompassing a broad spectrum of scales (spatial and temporal), from common machine, instrument and tool elements (such as a ball bearing and its race groove, a pair of spur gear involute teeth, cams and shafts and the components of polishing, machining and patterning instruments), to high-density data storage devices (e.g. read/write heads and recording media at nanoscale proximity), micromachines and certain biotribological systems (such as synovial joints).

Experimental and theoretical explorations of tribological processes (dating back to antiquity [14]), aiming at understanding their origins and at designing ways and means for minimizing losses related to such processes, employed until quite recently macroscopic observations and were anchored in treatments using continuum elasticity and contact mechanics [2]. The quest to observe and understand natural phenomena on refined microscopic scales and the everlasting trend toward miniaturization has led to the development of experimental and theoretical methodologies and devices that allow the interrogation of materials with increasing resolution. Such endeavors are enabled by the advent and proliferation of microscopies and local probes with atomic-scale spatial resolution (particularly tip-based microscopies such as scanning tunneling (STM) and atomic force (AFM) microscopies [15] and the surface force apparatus (SFA) [6]). In conjunction with improved understanding of the nature of cohesion and bonding in materials and formulation of new computational techniques and computer-based simulation methods, and coupled with the introduction of new computer technologies and large-scale computational strategies, these methodologies open new avenues of investigations of the microscopic origins of materials phenomena in general, interfacial processes in particular, and allow direct confrontation of experimental observations with theoretical predictions [2].

In this article, we focus, by way of examples, on computer simulations, where the evolution of a physical system is simulated, with refined temporal and spatial resolution, via a direct numerical solution of the equations of motion (classical or quantum). Using such methodologies, which serve as "computational microscopies", allows theorists to help explain and elucidate results of specific experiments, guide the developments of concepts, principles and theories unifying a range of observations and predict new behavior. Indeed computer simulations have been instrumental in the emerging field of nanotribology pertaining to the atomic and molecular scale origins of friction, lubrication and wear and the properties of nanoscale systems. Certain aspects of formation and properties of nanoscale solid interfacial junctions (the first and second examples given in the opening paragraph) are discussed in Section 2 and some issues pertaining to lubrication by liquids confined in nanoscale narrow junctions (the third example) are addressed in Section 3.

2. HARD JUNCTIONS – NANOWIRES

Junctions are materials structures which form upon bringing bodies into proximal interaction, during the separation of contacting bodies, or in the process of extension (e.g. pulling) of a material system. Past, as well as intensifying current, investigations of junctions have been motivated by the ubiquity of circumstances in which they may be formed; either naturally in the course of a physical process (as in the case of materials surfaces brought to close proximity to each other), or intentionally [12] (e.g. controlled generation of wires via the extension of materials contacts, as in the case of surface manipulations using tip-based methods, a break-junction technique, or by separation of wires in contact).

It is a common experience that the (tangential) force required to slide a macroscopic body on a surface is proportional to the load (the force, L, on the body in the normal direction to the sliding plane) regardless of the shape of the block and the sliding velocity. This is expressed by Amontons' law of friction as $F = \mu L$ (where ì is the friction coefficient). Amontons' law is a direct consequence of the Bowden and Tabor "plastic junction" theory of friction [16].

This model was stimulated by a number of observations including measurements of the electrical conduction between metallic surfaces in contact where it was found both under stationary and sliding conditions that the conduction is proportional to the load pressing the two surfaces together [17]. The model states that the total observed friction force, F, consists of two contributions: one called the adhesion term is the force to shear

intermetallic junctions formed at the regions of real contact between the two surfaces and the other originates from ploughing (which we are going to neglect here). When two metal surfaces are placed in contact they touch only at the tips of their asperities and at these regions the pressure may exceed the yield pressure of the metal (penetration hardness), σ_c, resulting in plastic deformation until the area, ΔS_r, in each such region (junction) is just large enough to support the load applied on it, i.e. $\Delta S_r = \Delta L/\sigma_c$. If the junction is characterized by a critical shear strength τ_c (i.e. the critical yield shear stress), the force to shear it (the friction force F) is given by $\Delta F = \tau_c \Delta S_r = \mu \Delta L$, where the friction coefficient $\mu = \tau_c/\sigma_c$ (note that μ is determined here by two materials characteristic parameters which are often of similar magnitudes). Amontons' law results from integrating over all the asperity junctions in the contact (the integrated area over ΔS_r is called the real (or true) area of contact and it is much smaller than the apparent one).

But what happens under conditions when the deformations are mainly elastic, since then ΔS_r (and thus the total real multi-asperity area of contact) will vary nonlinearly with load (e.g. $\propto L^{2/3}$ using the original contact mechanics of Hertz [18])? Interestingly, when assuming that the asperities are distributed in height about some mean value (and for a probability distribution function which decays sufficiently fast, such as a Gaussian or an exponential) and averaging over that distribution, a linear dependence on L of the total real area of the contact is recovered [19] and thus Amontons' law follows. However, what if there is only one such asperity (as is the case with a carefully prepared AFM tip) and furthermore when the size of the junction is in the nanometer range? Here we enter the reduced size regime where simple scaling may not be expected to, and often does not, apply.

Prior to discussing in more detail formation mechanisms and certain properties of nanowire junctions I would like briefly to comment on electrical conduction measurements which as mentioned above have long been used in tribological investigations to provide a measure of the real area of contact between materials. Analysis of such measurements employed the (Maxwell [20]) electrical conductance $G = 2r_0/\rho$, where r_0 is the radius of the circular contact junction and ρ is the electrical resistivity of the material (note that G is proportional to r_0 rather than to r_0^2). This expression for G is valid only when the electron (elastic) mean free path (l) is smaller than the radius r_0 (the so called diffusive transport regime). For ballistic (i.e. $l \gg r_0$) point contacts (between bulk reservoirs) with r_0 in the submicron range (but larger compared with the electron's wavelength), the conductance is determined by Sharvin's (semiclassical)

expression [21] $G = (2e^2/h)(k_F r_0/2)^2$. Furthermore, in nanoconstrictions (nanowires) connecting bulk reservoirs, with $l \gg r_0$ and $r_0 \sim \lambda_F$, the ballistic electronic conductance exhibits quantum effects, such as stepwise variation of G in units of the conductance quantum $2e^2/h$ (where $h/2e^2 \sim 12.9$ kΩ) as the transverse size of the constriction is varied. This phenomenon originates from the discrete character of the change in the number of conducting channels (number of transverse electron states below E_F) transmitted through the constriction upon variation of its transverse size. Here the conductance measured between the reservoirs connected by the nanowire is given (at zero temperature) as

$$G = (2e^2/h)\sum_{i,j} T_{ij}(E_F)$$

where T_{ij} is the probability of transmission from the j-th incoming channel at one end of the wire to the i-th channel at the other end [10–12]. More will be said on this topic in what follows.

Formation mechanisms and mechanical properties of interfacial nano-scale junctions (in the form of ordered crystalline three-dimensional nanowires) have been predicted through early molecular-dynamics simulations [22], where the materials (a gold surface and a nickel tip and vice versa) were modeled using semiempirical embedded-atom potentials. In these studies it has been shown that separation of the contact between the materials (formed initially upon bringing them into close proximity or via nanoindentation) leads to generation of a connective crystalline junction that elongates and narrows through a sequence of structural instabilities [22–24]. At the early stages [Fig. 1(a)], of elongation of the junction accumulated stresses induced by pulling may be distributed in various regions of the wire and a large number of glide planes (mainly (1 1 1)) with variable dimensions are involved in multiple slip events. At later stages, when the lateral dimension of the connective wire necks down to a diameter of about 10–15 Å, the number of active glide planes decreases [Fig. 1(b)] and further elongation involves a succession of stress accumulation and fast relief stages associated with a sequence of order-disorder structural transformations localized to the neck region [see Fig. 1(c)]. The structural evolution patterns have been shown through the simulations to be portrayed by oscillations in the force required to elongate the wire [Fig. 2(a)] and in the axial component of the stress tensor [Fig. 2(b)]. At the later stages of the elongation process these oscillations exhibit a regular pattern with a period of about 2.5 Å which is close to the interlayer distance between (1 1 1) layers (see $\Delta z \geq 35$ Å in Fig. 2(a,b), i.e. when the radius of the narrowest constriction of the wire is reduced to about 10 Å). On the other hand, for the thicker wire (i.e. $\Delta z \leq 35$ Å) the force and stress

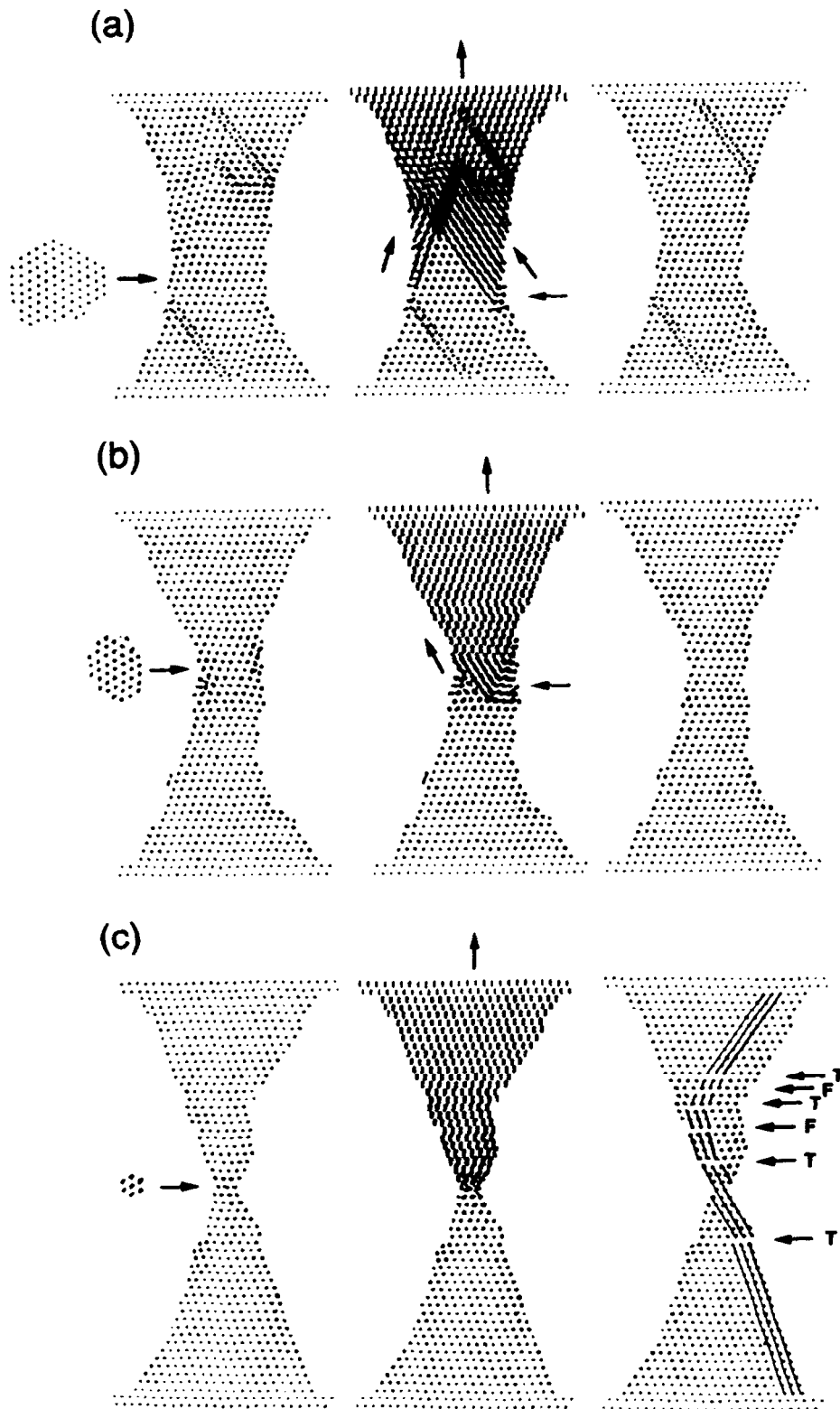Fig. 1. Side views of atomic configurations and short-time trajectories in 5 Å thick vertical slices through the wire, recorded (a–c) during the elongation stages (i)–(iii) marked in Fig. 2(a), respectively. In each stage the left and right frames correspond to before and after configurations and the central one corresponds to the brief structural transformation stage; the arrows in the middle frames of (a) and (b) denote the glide directions. For the final configuration in (c) fault (F) and twin (T) planes are marked (lines along atomic rows are drawn to guide the eye). Included also in (a–c) are top views of the narrowest cross-sections of the wires, before the elongation step.
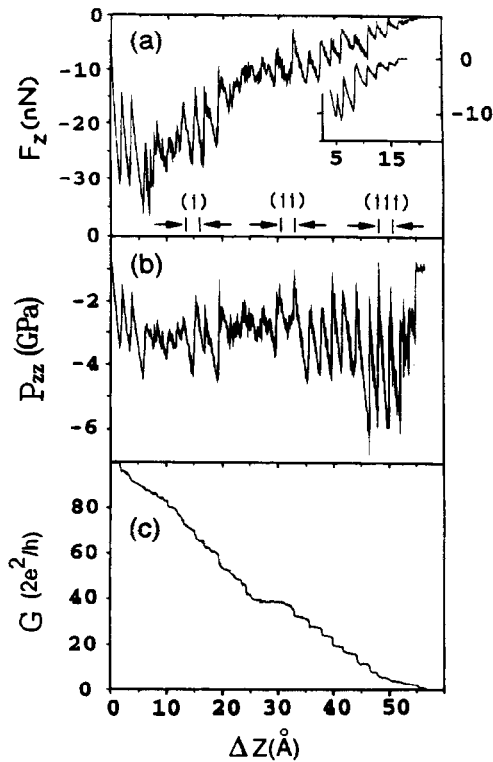
Fig. 2. F_z, in nN, shown in (a), axial component of the stress tensor P_{zz} in GPa, shown in (b) and calculated conductance G, in unit of $2e^2/h$, shown in (c), plotted vs displacement Δz, in Å obtained from room-temperature MD simulations of the elongation of a large (1 1 1)-oriented gold wire (initially equilibrated as a 30-layer wire with a ~ 17 Å radius of its narrowest cross-section). The displacement intervals marked (i)–(iii) correspond to those for which atomic configurations are shown in Fig. 1(a–c), respectively. Shown in the inset is the force (F_z in nN) recorded in a separate simulation of the elongation process of smaller Au(1 1 1) wire (equilibrated initially as a 16-layer wire with a radius of ~ 10 Å at its narrowest cross-section). The displacement scale for the shorter wire was positioned with respect to that of the longer one such that at its start the radii of the narrowest cross-sections of the two wires achieved very close values. This comparison serves to illustrate the approximate invariance of the properties of nanowires formed during elongation of junctions with respect to the initial sizes of the junctions.

oscillations are quite irregular with large variations in the oscillation amplitudes and periods.

We also observe that the structural transformations of the wire can lead to generation of stacking faults and/or twin-boundaries [see for example Fig. 1(a)]. Such defects may anneal during the structural evolutions of the pulled wire [compare Figs 1(a) and 1(b)] and some may be present in the ultimate stretched nanowire (see Fig. 1(c) where faults and twin-boundaries, denoted by F and T, respectively, are seen).

The critical resolved yield stress of gold nanowires has been predicted from the simulations [22, 25] to be ~ 4 GPa, which is over an order of magnitude larger than that of the bulk and is comparable to the theoretical ("ideal") value for Au (1.5 GPa) in the absence of dislocations. The mechanical ideal nature of nanowires (and nanoscale systems in general) is another instance where reduction in system's size is associated with the emergence of new behavior (here mechanical response) and where "small is different" in a fundamental way. A simple argument explains the energetics underlying this phenomenon. In metals of size scales larger than the average separation between two neighboring dislocations plastic deformation occurs via motion of dislocations, resulting in significant lowering of the critical yield stress from its ideal value (e.g. for a cubic crystal the ideal shear strength is $\sim G/2\pi$ where G is the shear modulus). However, for a nanoscale junction, e.g. made of gold, with $R \sim 10$ Å, the pressure needed to generate a dislocation loop with this radius (e.g. for gold ~ 5 GPa) may greatly exceed the macroscopic yield stress of the material. Thus, plastic deformation of nanometer scale metals (and other materials) may occur through dislocationless mechanisms with consequent increased strength.

To first approximation ballistic conductance through the nanowire is determined mainly by the dimension and shape of the narrowest constriction (i.e. the number of conducting channels is given by the number of transverse electronic states at this region and their degeneracies) and it may be estimated via the semiclassical modification (Weyl's correction) of Sharvin's expression, [26] $G = (2e^2 h)[S(0)k_F^2/4\pi - L(0)k_F/4\pi]$, where $S(0)$ and $L(0)$ are the area and perimeter of the narrowest cross-section of the nanowire. The conductance shown in Fig. 2(c), calculated in this way, exhibits stepwise variations, which at the later stages of the elongation are characterized by well-defined plateaus and steprises. Additionally, the variations in the conductance correlate with the oscillations of the force, which portray the structural evolution of the wire. In more refined calculations using the Landauer formalism [27, 10, 11] the conductance of such nanowires, at the ultimate stages of elongation, is often found to vary in a quantized manner in units of the conductance quantum $2e^2/h$ [28, 29]. Note however that significant roughening of the wire surface as well as defects such as the stacking faults and twin boundaries mentioned above may influence the ballistic transport of electrons through the wire. The onset of ballistic transport in nanowires (i.e. when electron mean free path is larger than the length of the wire) and quantization of the conductance when the transverse dimension of the wire approaches a length scale comparable to the electron's Fermi wavelength are

the origins of the failure of the simple scaling with size valid for Ohmic conductors.

These predictions, as well as anticipated electronic conductance properties [22], have been corroborated in a number of experiments using scanning tunneling and force microscopy, break junctions and pin-plate techniques at ambient environments, as well as under ultrahigh vacuum and/or cryogenic conditions [28]. Particularly interesting are experimental (room temperature) observations of the oscillatory behavior of the elongation forces and of direct correlations between the step-wise changes in the conductance and the force oscillations [30] (portraying the predicted structural evolution), measurements of critical yield stresses of 3 to 6 GPa for Au nanowires [30, 31], as well as theoretical [25] and experimental [25, 30] observations of mechanical and structural reversibility in elongation-compression cycles of nanowires, reflected also in measured and calculated conductance traces of nanowires undergoing such mechanical cycles and correlated with the predicted [22] dislocation-less nature of the mechanical response of such systems.

Computer simulations have also revealed the nature of mechanical and structural response of nano-scale junctions formed between a tip and a surface when they are sheared [23, 32, 33]. For example, shearing of a nanowire junction formed between a nickel tip and a gold surface occurred between the gold layer adherent to the nickel tip and the layer underneath it and proceeded in a "racheting" (atomic-scale stick-slip) manner, reflected in the recorded forces on the tip which oscillate as atomic rows in the layers pass each other. From the magnitude of the forces and the contact area between the sliding layers we estimate the shear strength of such junction as ~ 2 GPa [23]. The magnitude of the frictional shear resistance depends on the sliding direction and registry between the sliding layer.

One of the most fascinating aspects of nanowires is the prospect of formation of atomic-scale contacts and switches, which may occur towards the ultimate stages of elongation [22, 34] (that is before complete physical separation, or breaking, of the wire). Understanding of the atomic arrangements and structural evolution, electronic properties and dynamics of such nano-junctions, particularly as they approach the "one-atom contact" regime, is a significant challenge requiring a detailed theoretical description based on first-principles electronic structure calculations. To this end we have used first-principles molecular dynamics simulations for sodium wires [34], where the dynamics of the ions (with an integration time-step of 3 fs) evolves at finite temperature $(T = 190$ K) on concurrently calculated ground-state potential energy surfaces, evaluated self-consistently for each ionic configuration using the local-spin-density

functional theory, in conjunction with non-local norm-conserving pseudopotentials.

The simulation starts from a sodium block of bulk body-centered cubic, b.c.c., (1 0 0) layers oriented along the z-axis and tapered to a narrowing in the middle. After equilibration of the initial wire configuration, measuring 19.98 Å, 19.98 Å, 21.3 Å in the (x, y, z) directions, the structure of the junction was mostly b.c.c., except in the middle layer [Fig. 3(a)]. Each subsequent elongation involves a uniform dilation in the z direction, followed by dynamical equilibration for several picoseconds (at the start of the equilibration period stochastic thermalization to 190 K was used).

The atomic configurations of the sodium wire at selected stages of elongation shown in Fig. 3 reveal development of cluster derived structures (cds) at the narrow-neck region. Particularly striking is the formation of a 13-atom (slightly distorted) icosahedron (5-fold symmetric), supported between the upper and lower parts of the wire [Fig. 3(b,c)]; this structure may also be viewed as two Na_7 pentagonal bipyramidal (pbp) clusters sharing an apex atom. Subsequent elongation results in "opening" of the structure [Fig. 3(d)] and stretching of the contact past this stage results in formation of a pbp Na_7 cluster (top) bonded through one of its apex atoms to the upper atom of a tetrahedral cluster (bottom), giving the appearance of a stretched sodium dimer at the narrowing [Fig. 3(e)]. Further elongation results in breaking of the nanowire [Fig. 3(f)]. The occurrence of these molecular-like supported structures which correlate with those derived for *isolated* sodium clusters, suggests that in atomic-scale narrow contacts the atomic coordination and nature of bonding may be described using information from investigations pertaining to small (isolated) clusters. In a certain sense the reduced dimensions, increased surface to volume ratio and atomically impoverished environment in such nano-scale solid-state junctions provide a link to the realm of finite-size cluster science, where ground-state (and isomeric) structures different from the bulk and "magic numbers" (that is enhanced stability of certain sequences of cluster sizes, shapes and structural motifs due to electronic and/or geometric-packing shell effects, which may vary from one class of materials to another) are known to occur [35–37].

Contour plots of the self-consistent local effective potential confining the electrons to the wire are shown in Fig. 4 for the 23.97 Å and 29.96 Å wire configurations [compare Fig. 3(b and e)]. These confinement potential profiles outline the shape of the wire; note the rather "smooth" appearance of the "effective potential tube" (defined by the peripheral outmost solid contour corresponding to the Fermi energy), as a result of effective screening; the approach of the confining potentials to the
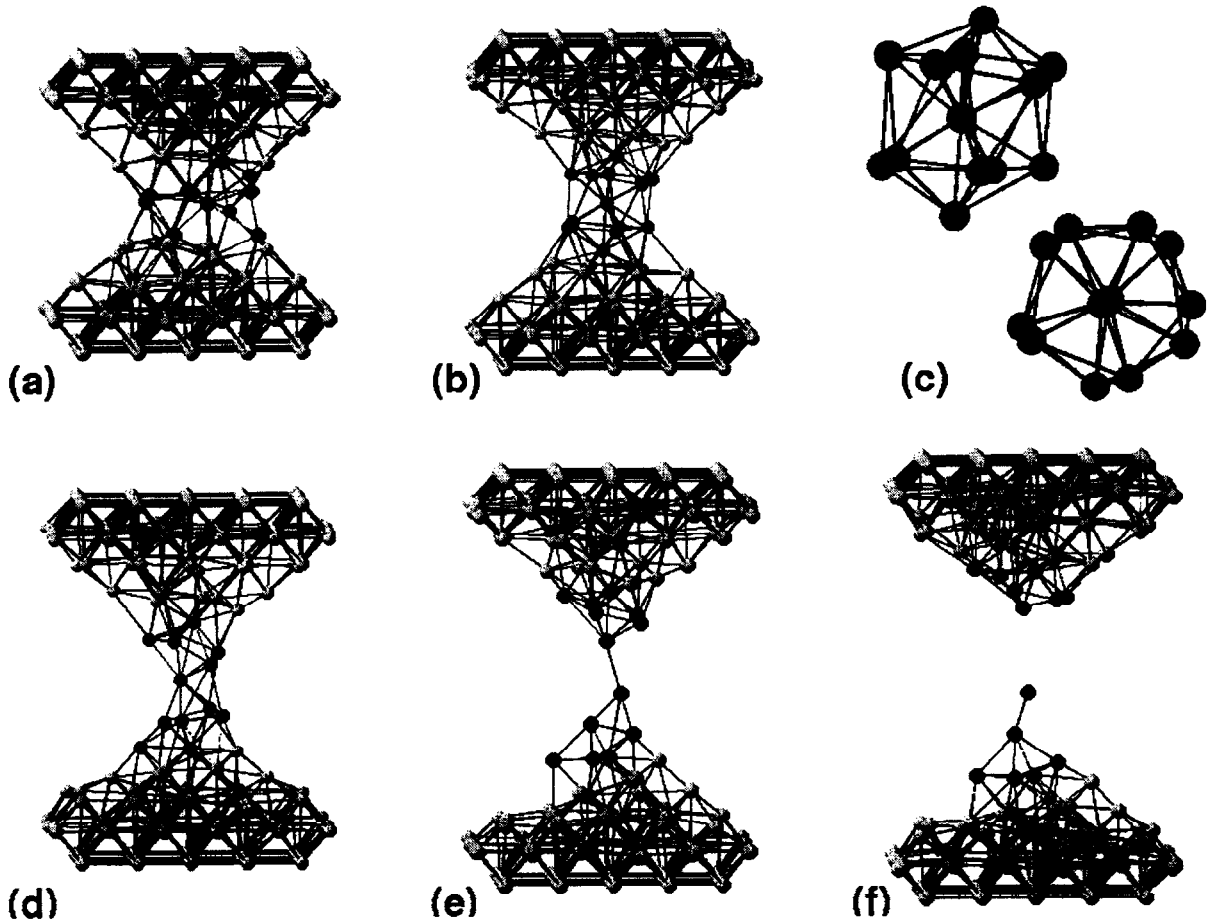
Fig. 3. Atomic configurations of a sodium nanowire at selected elongation stages, obtained through first principles MD simulations. The configurations in a, b, d, e and f correspond to wires of lengths 21.3 Å, 23.97 Å, 26.64 Å, 29.96 Å and 31.96 Å, respectively. In (c) side and top views are shown of the stretched icosahedral supported cluster (see neck region in (b)). The 13 atoms forming the icosahedron are distinguished also by color in the other configurations to allow visualization of the structural evolution.

vacuum level (beyond the outer dashed contour) is similar for both wires, indicating a reduced screening in the more elongated one. In this context we note the close-to-circular shapes of the confining potentials at the narrowing (particularly as the wire narrows, see right-hand panels in Fig. 4), which correlates with the conductance quantization pattern [38] reported for sodium wires [39].

The time averaged global and local (in the narrowing) electronic densities of states (DOS) obtained from a dynamical simulation at 190 K of the nanowire corresponding to the selected configuration shown in [Fig. 3(b)], is displayed in Fig. 5(a), along with the time-variation of the DOS at the Fermi-level, $(N(\epsilon_F)$ in Fig. 5(b)). We observe that while both the global and local $N(\epsilon_F)$ are finite, indicating metallic character, they exhibit significant fluctuations on a subpicosecond time scale [Fig. 5(b)], originating from redistribution of the

electronic energy levels caused by ionic motion. Obviously, such fluctuations are expected to be portrayed in the electronic transport through the nanowire.

Using the density-functional Kohn–Sham (KS) orbitals the electronic conductivity can be calculated from the linear-response (Kubo) formula [34, 40], yielding for the time-averaged conductance (extrapolated to the d.c. limit) of the 23.97 Å nanowire $\langle G \rangle = (5.2 \pm 0.7)g_0$, where $g_0 = 2e^2/h$ $(g_0^{-1} = 12.9 \text{ k}\Omega)$. Similar analyses yield conductance values of (11.0 ± 1.5) g_0 and (1.2 ± 0.3) g_0 for the 21.3 Å and 26.64 Å wires [Fig. 3(a) and 3(d)]; for the 29.96 Å wire [Fig. 3(e)] a value much smaller than 1 g_0 is obtained. The conductance shows an expected decreasing trend as the wire narrows; we note here that no attempt has been made here to search for wire configurations (that is elongations) which may yield a particular sequence of conductance values.
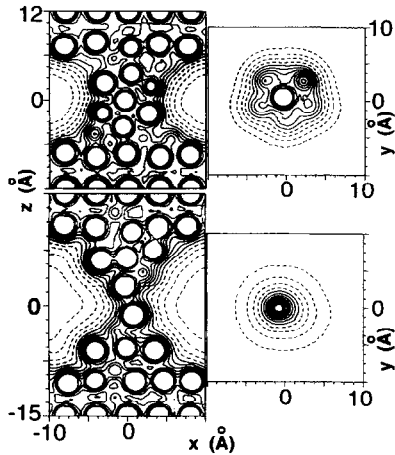
Fig. 4. Contour plots of the local part of the self-consistent LSD effective potentials corresponding, respectively (top and bottom), to the wire configurations shown in Figs 3(b) and 3(e); contours inside the repulsive atomic cores, where the non-local contribution is significant, are not shown. On the left contours are in the plane containing the axis (z) of the wire and on the right they are drawn in the transverse plane at the narrowest part of the wire. All contours correspond to energies below the vacuum level, with the outermost solid ones corresponding to ϵ_F.

In light of our aforementioned observation of temporal fluctuations in $\rho(\epsilon_F)$, caused by finite-temperature dynamical structural fluctuations, we display in Fig. 5(c) the corresponding calculated time variations of the conductance G (whose time-average yields the aforementioned value of 5.2 g_0). The resonance-like features in G correlate with the temporal structural and electronic spectral fluctuations (in both the local density of states and momentum matrix elements) due to thermal vibrations. Such finite-temperature effects and factors related to the "non-ideal" (structural) nature of the nanowires underlying scattering of the electrons, as well as inherent irreproducibility in the fabrication of nanowires through contact elongation or break junction techniques, are likely to be the source of the distribution of measured conductance values (commonly displayed as conductance hystograms of G). Consequently, these results suggest that dynamical conductance fluctuations may be of importance in considerations pertaining to atomic-scale contacts and that fast spectroscopical measurements of electronic transport in nanowires may provide significant insights into cluster-derived atomic arrangements and dynamics in such nano-scale solid-state structures.

The above prediction of the occurrence of supported cluster-derived cluster configurations of enhanced stability in nanowires, led most recently [41, 42] to the suggestion that upon elongation such wires exhibit
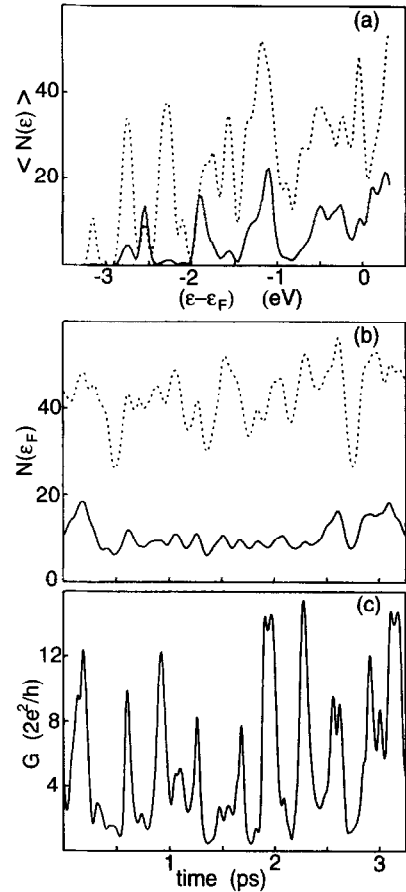

Fig. 5. Spectral and conductance characteristics for the 23.97-Å nanowire [Fig. 3(b)]. (a) Time averages (from simulations at 190 K) of the global (dashed line) and local (solid line; evaluated at the narrowmost, cluster, region) densities of states, (N(ϵ)). (b) Time variations of the global and local DOS at ϵ_F. (c) Time variation of the conductance G, showing sub-picosecond fluctuations, with an average value of (5.2 ± 0.7) g_0. The Kubo conductivity formula used in our calculations has been discussed previously [40] and its use in conjunction with finite-temperature simulations alleviates to a large extent some of the issues discussed there. In our calculations the delta-function is represented by a gaussian with a width of $\zeta = 0.0163$ eV ($\zeta/k_B = 190$ K), which is equal to half the average level spacings near ϵ_F. Larger broadening decreases, but does not obliterate, the magnitude of the conductance fluctuations.

a self-selection of a (discrete) sequence of stable "magic wire configurations" (MWCs), which in jellium modeled wires correspond to a sequence of "magic" wire radii. Indeed, model calculations on metallic nanowires (using density functional theory in conjunction with a shell-correction method, developed earlier in studies of the electronic shell structure and shape variations of metallic clusters [36]) have shown that the total energy of such nanowires exhibits an oscillatory pattern as a function of the wire's length (or radius, for volume

conserved wires) with local minima corresponding to MWCs.

Such oscillatory pattern originates from quantization of the electronic spectrum, that is, formation of electronic energy subbands (exhibited as oscillations (cusps) in the density of states of the wire [42]) caused by the reduction of the radius of the metallic nanowire to the order or the electron's Fermi wavelength. This reorganization (quantization) of the spectrum is analogous to that known in other fermionic systems of reduced dimension [36], such as zero-dimensional metal clusters, atomic nuclei and ^{3}He clusters and would occur also in two-dimensional nanoscale thin films. Indeed self-selection of size, shape and form are characteristic to the nanoscale realm and are exhibited in both quantum and classical systems (see e.g. the discussion on layering of liquids confined in nanoscale junction in Section 3).

Furthermore, the aforementioned oscillatory pattern in the total energy of nanowires vs their length (or radius) leads directly to oscillations in the force required to elongate the wire and to correlated stepwise variations of the (ballistic) conductance in units of $2e^2/h$. These patterns and the correlation between them have been shown both numerically and through a semiclassical analysis [42] (reminiscent of periodic orbit theory) to be dominated by the quantized spectrum of the transverse states at the most narrow part of the constriction in the nanowire.

3. SOFT JUNCTIONS

If you were persuaded after reading the preceding section that nanoscale hard (solid) nanowire junction are physical objects of interest well deserving to be pursued on their own merits, you may be somewhat disappointed to learn that much research in nanotribology focuses on designing ways for preventing their formation altogether through surface coatings and ultrathin film lubrication. However, understanding the structure, dynamics and rheology of ultrathin films (of nanometer scale thickness) of low molecular weight hydrocarbons adsorbed on solid surfaces and in particular of such films confined between solids, is of fundamental interest as well as practical importance for many processes, such as lubrication, adhesion, coatings, chromatography and membrane separation. Indeed, the properties of such systems have been the subject of numerous investigations (for recent reviews see [1–9]) employing sensitive microscopies (the surface force apparatus (SFA), atomic force microscopy (AFM), friction force microscopy (FFM) and a quartz microbalance technique [9]), as well as computer simulations and other theoretical approaches.

One of the major issues of modern research in this area pertains to the dependencies of the properties of thin confined complex molecular films (e.g. short to medium length alkanes and polymers) on the nature of the constituent molecules (e.g. molecular weight, straight vs branched chains) and correlations between their response to external parameters (e.g. degree of confinement, load, shear rate) and molecular characteristics. Such issues are of fundamental interest, as well as of significance for formulation of molecular-scale-based technological design principles.

Confined fluids have been observed experimentally and theoretically to exhibit unique structural, dynamical, mechanical and rheological properties, different from those of the bulk and dependent on the degree of confinement (load), operational conditions (e.g. shear rate and temperature) and nature of the fluid (e.g. molecular shape, size and complexity) and its interactions with the boundaries (e.g. chemical or physical binding) [1]. A central property of liquids confined between solid boundaries which are smooth on the molecular scale (as well as of films adsorbed on a solid surface) is their tendency to organize into layered structures characterized by load sustaining capacity [1, 6], where the mean local density of the liquid oscillates with distance normal to the boundaries. This property is portrayed by oscillatory (solvation) forces between confining surfaces [6] (that is, oscillations in the force between the confining boundaries as the distance between them, i.e. the confining gap width, is varied, with a period approximately equal to the width of the film molecules). Such oscillatory forces were observed and simulated (see citations 1–3 in [43]) for simple liquids (e.g. modeled as spheres) and non-polar globular molecules (e.g. octamethylcyclotetrasiloxane, OMCTS, which is a globular molecule with an about 9 Å diameter), as well as for complex liquids such as straight-chain alkanes (e.g. n-hexadecane, n-C$_{16}$H$_{34}$ and tetracocane, n-C$_{24}$H$_{50}$) and polar liquids (e.g. water).

While the layering of confined films and solvation force oscillations are related, the distinction between these two phenomena should be emphasized [6]. Recent simulations [44, 45] revealed that the measured strong attenuation of force oscillations in squalane films (a branched alkane, 2,6,10,15,19,23-hexamethyl-tetracosane) in comparison to those found for films of globular molecules and straight-chain alkanes (n-hexadecane and n-tetracosane), is not correlated with reduced layering in the branched molecular films. Rather, the difference in solvation force characteristics between the branched and straight-chain (as well as globular) molecular films originates from different modes of response in these systems to variation of the degree of the confinement (as well as under shear), with the former (e.g. squalane) responding in a more liquid-like manner compared to globular and straight chain

alkanes and thus squalane is predicted to be a preferred lubricant; at first this appears rather strange since in the bulk the viscosity of a liquid made of a branched alkane is higher than that of a straight chain alkane with a similar molecular weight — but such is the effect of the high degree of confinement.

Confined ultrathin films may exhibit different response modes, in shear [46, 47] as well as in response to variation of the normal distance between the confining surfaces [48]); a liquid-like response in which the liquid responds to the deformation by flow, or spreading (as in drainage measurements [49, 50]) and a solid-like response characterized by observation of the development of "yield stress" in the confined fluid [48, 51]. Furthermore, when the opposing solid boundaries are set in shear motion with respect to each other, through pulling at constant velocity on a spring attached to one of the confining blocks, their motion may exhibit stick-slip character for a certain range of velocities with a transition to steady sliding at higher velocities and eventually transforming into a state with ultra-low kinetic friction (the so-called superkinetic regime) for velocities exceeding a critical one (v_c) [52].

Some of the properties of confined fluids are illustrated here through simulations of globular molecules (modeled as Lennard-Jones spheres [43]), using a recently developed [44, 45] grand-canonical molecular dynamics (GCMD) method (i.e. a constant chemical potential (μ), pressure (P) and temperature (T) ensemble); for simulations involving straight and branched-chain molecules see [44, 45, 53]. In these simulations, the fluid (spherical) molecules were treated dynamically using Lennard–Jones (LJ) interactions, with parameters, corresponding to a commensurate (C) solid-liquid system; i.e. corresponding to the confining solid and the bulk liquid having the same density at the temperature of the simulations which is above the melting temperature of the bulk material at $P = 1$ atm. Similar simulations of the equilibrium properties were performed also for the same liquid but confined by crystalline solid boundaries with a lattice constant which is incommensurate with the size of the molecules; this will be referred to as the incommensurate film (IC).

For widths of the gap between the confining solid surfaces $D \leq 30$ Å, the confined C liquid organizes into layered structures normal to the solid boundaries [43], see Fig. 6 (similarly for the IC film [44], not shown here). The degree of ordering into such layers depends on D and it originates [43–45] from variations in the internal energy and entropic contributions to the free energy which oscillates (as well as the corresponding solvation forces) as a function of D.

Narrowing of the gap results in expulsion of molecules from the confined region ("squeezing-out" of the film and transition to a film with a smaller number of layers
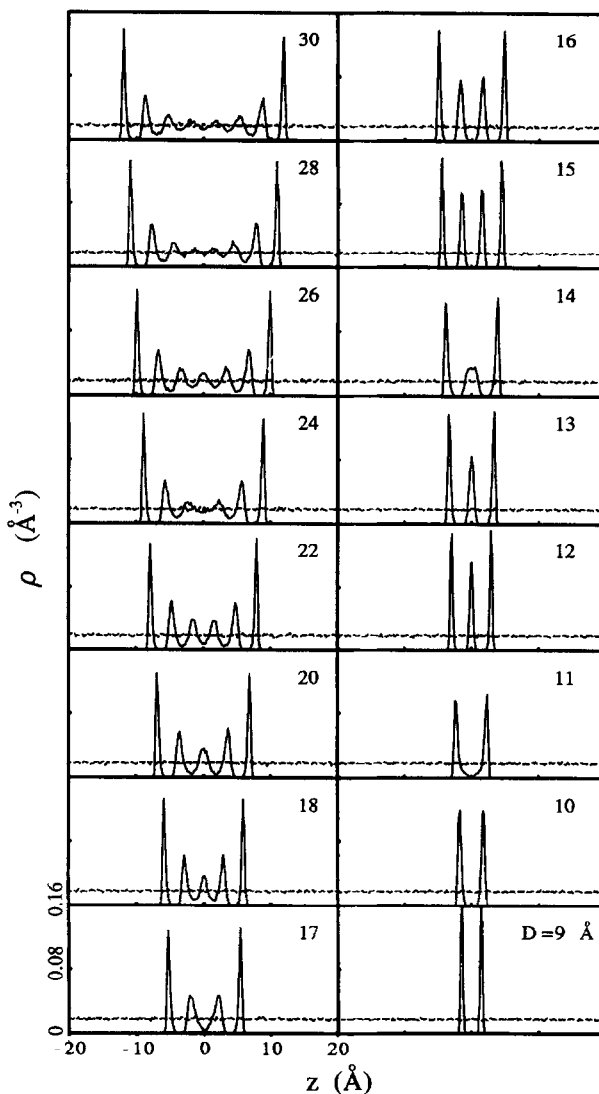

Fig. 6. Equilibrium density profiles for the commensurate film along the z direction (normal to the confining solid surfaces); solid lines correspond to the film in the confined region and the dashed lines calculated for the region outside the gap. The gap widths (D) for which the profiles were calculated are indicated. Note that the liquid density outside the confinement (dashed line) is uniform and remains constant for all values of D, while the layered density features in the confined film (particularly in the middle region of the film) vary in sharpness depending on the degree of confinement.

occurring with a periodicity of about 3.5–4.0 Å. Sharp, well-formed layered configurations (with similar layer densities) in the C film occur for a sequence of gap width (e.g. $D = 26, 22, 18, 15, 12$ and 9 Å, corresponding to 7, 6, 5, 4, 3 and 2 layers, respectively, see Fig. 6), with a lower degree of interlayer order for intermediate gap widths; in the IC film the well-formed layers occur for similar values [44].

The layering transitions in the confined films are portrayed [Fig. 7(a)] in solvation force oscillations with the local positive force maxima corresponding to configurations with well-formed layers and the amplitudes of the force oscillations $f_z(D)$ (i.e. the total force exerted by the interfacial film on the containing surfaces) somewhat larger for the C film. In these configurations we find also
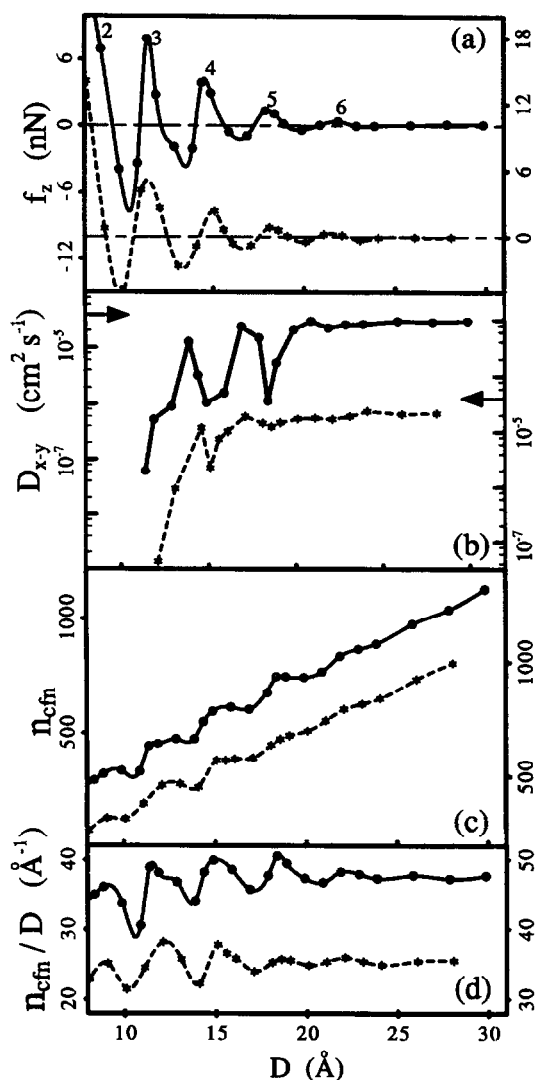
a high degree of intra-layer order (hexagonally close-packed) which becomes sharper upon increased confinement [43] and is higher in the C film which is in epitaxy with the solid surfaces; the degree of intra-layer order reduces for intermediate states between well-formed configurations.

Further insights into the layering transition processes are obtained from records of the number of segments in the confined region, n_{cfn} (as well as n_{cfn}/D), plotted vs the distance between the confining surfaces (D), shown in Fig. 7(c). The variation of n_{cfn} exhibits a step-like pattern with sharp drops in the number of confined molecules occurring for the transition from an n-layer film to an $(n-1)$-layer one (resulting from expulsion of approximately a layer-worth of molecules into the surrounding liquid), with the steps becoming sharper as n decreases (note that the pattern extends for the C system to a larger value of D). For each of these transitions the drop in n_{cfn} is caused by a relatively small reduction ($\sim 0.5-1$ Å) of the gap width from that corresponding to an initial well-layered configuration of the film (i.e. the number of layers in the film at the bottom of each step is decreased by one from that corresponding to the film at the top of the step (and the plateau). These transitions and the accompanying diffusion [Fig. 7(b)] and shear-response characteristic of the C film (which was found to develop solid-like shear moduli starting from the well-formed 5-layer configurations) correlate with recent SFA measurements on films of globular molecules (OMCTS) confined by mica surfaces [48], where a rather abrupt transition into a solid-like state has been reported for a 6-layer thick film. We remark here that similar step-wise patterns in n_{cfn} were also found for straight-chain alkanes but not for a branched one (squalane) correlating with the aforementioned liquid-like character of the latter under high confinements.

3.1. Friction control

Underlying the aforementioned dynamical properties of confined molecular films and their rheological response are microscopic momentum and energy transfer mechanisms governed by couplings between the lubricating film molecules and the (mechanical) motion of the shearing boundaries, as well as between intra- and inter-molecular degrees of freedom. Associated with such couplings is a spectrum of characteristic times (τ_r) (materials, temperature and load dependent) for dynamic structural (and conformational) relaxations and energy redistribution and dissipation, as well as system characteristic times (operationally dependent) such as the mechanical drive-time $\tau_{drive} = \lambda/v$, which is the time for driving the systems at a velocity v a characteristic distance λ. The ratio $D_e = \tau_r/\tau_{drive}$ is defined as the Deborah number [55] and it is expected that different

Fig. 7. (a) Equilibrium solvation forces, f_z in nN, plotted vs the width of the confining gap, D in Å. (b) 2D diffusion constants, D_{xy} vs D, plotted on a logarithmic scale. Simulated values in the bulk liquid are denoted by arrows. Note particularly for the C film (solid line), the abrupt decrease in D_{xy} for the $6 \rightarrow 5$, $4 \rightarrow 3$ and $3 \rightarrow 2$ transitions in the number of layers. (c) Number of molecules in the confining gap, n_{cfn}, in (c) and n_{cfn}/D (proportional to the density in the confined region), in (d), plotted vs the gap width, D in Å. Results are for the C (solid line) and IC (dashed) confined LJ films, with the left and right ordinate, respectively.

regimes of rheological response correspond to different values of D_e, which may be accessed for a given lubricant (as well as given temperature and load) through control of τ_{drive}. Thus, it is expected that dissipation will be maximal for $D_e \sim 1$ and otherwise reduced friction will occur.

In the GCMD simulations of shear [54] the direction of sliding is along the y axis. In these simulations the upper solid block is connected to a horizontal (y) spring (spring constant $k_s = 0.8$ N m^{-1}) which is pulled at a constant velocity v_s. Such simulations were performed both under constant applied load p_{ext}^z and when the gap

width was modulated periodically in time using a triangular drive (modeling a time-varying externally applied load).

Results of constant load ($P_{ext}^z = 73$ MPa) shear simulations [54] of an equilibrated 4-layer (with ~150 molecules per layer) commensurate liquid film (see Fig. 9) for three spring-pulling velocities v_s are shown in Fig. 8. A characteristic stick-slip sliding motion is found for the lower velocity (1 m s^{-1}), approaching steady sliding for $v_s = 20$ m s^{-1} correlated with a notable decrease in the friction force (panels (b) in Fig. 8);
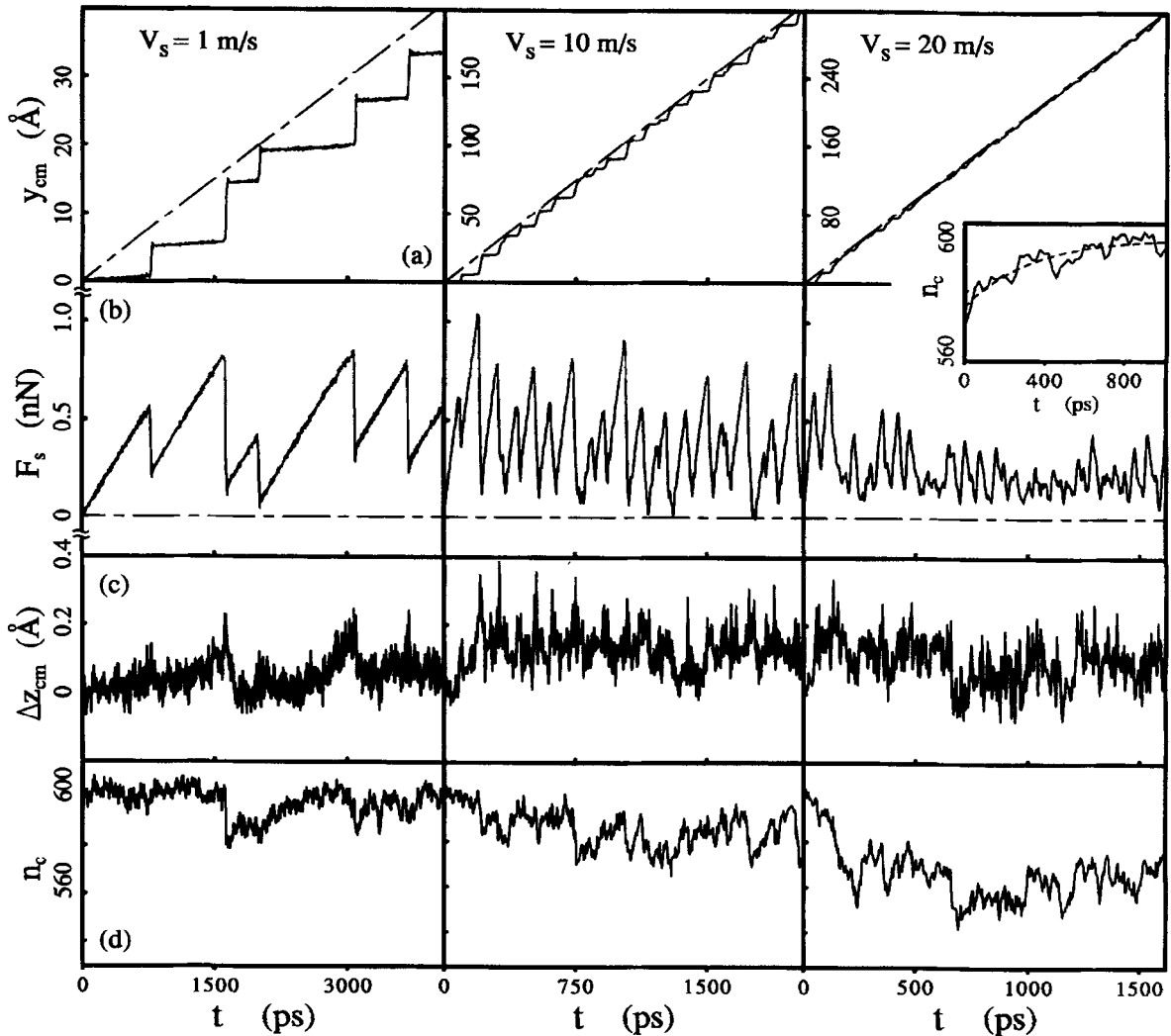

Fig. 8. (a) Position of the center of mass of the spring-pulled upper solid block (y_{cm}, solid line), (b) sliding-spring force (F_s), (c) height variations of top block (Δz_{cm}) and (d) number of molecules in the confinement (n_c), plotted vs time (t), obtained from GCMD simulations of a 4-layer junction under constant external load $P_{ext}^z = 73$ MPa, sheared with spring velocities of $v_s = 1$ m s^{-1}, 10 m s^{-1} and 20 m s^{-1} as indicated. The dashed line in (a) depicts $v_s t$. Note the stick-slip dynamics for $v_s = 1$ m s^{-1}, decreasing for $v_s = 10$ m s^{-1} and obliterated for $v_s = 20$ m s^{-1} (approaching the steady-sliding regime). In the inset in the top panels for $v_s = 20$ m s^{-1} we display the time evolution of $n_c(t)$ following a sudden cut (denoted here as $t = 0$) of the sliding spring during the steady-sliding. This information was used to estimate the molecular flow relaxation time, ϵ_f (the dashed line indicates an exponential fit with $\tau_f = 300$ ps). Distances, force and time in units of A, nN and ps, respectively.
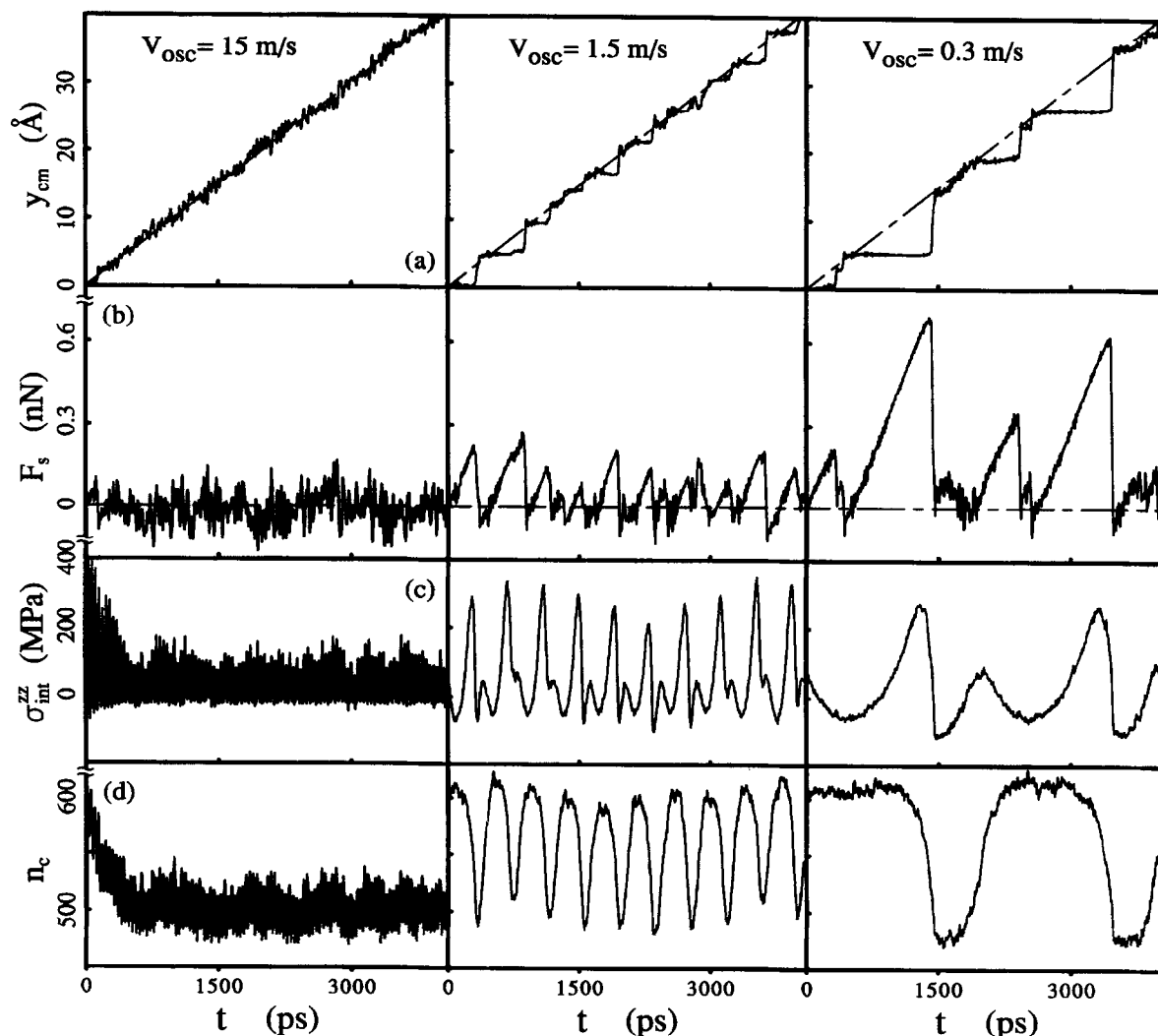
Fig. 9. Same as Fig. 8 with $v_s = 1$ m s^{-1}, but under directional oscillations of the top solid block along the z-axis (normal to the shear plane), using a triangular waveform with an amplitude of 1.5 Å and velocities $v_{osc} = 15$ m s^{-1}, 1.5 m s^{-1} and 0.3 m s^{-1}, as indicated. In panels (c) we display the time variations of the normal component of the internal stress on the confining boundaries, σ_{int}^{zz} (in units of MPa). Note the transition to a superkinetic regime for the highest oscillation velocity and the intermittent well-defined stick-slip and superkinetic dynamics for the lowest one.

from these observations we conclude that $v_\ell > 20$ m s^{-1}. Accompanying the stick-slip motion are sharp variations in the number of confined molecules, as well as small dilations of the gap width. On the other hand, the transition into a steady sliding regime is signaled by a sharp drop in n_c (see Fig. 8(d) for $v_s = 20$ m s^{-1}) with subsequent variations in the gap width and n_c being small and erratic.

The two stages in the stick-slip cycles and the transition between them are accompanied by structural changes in the film. Thus, while the film in the stick stages exhibits a dynamical phase characterized by a layered structure with high degree of intralayer order (both in the interfacial layers and inside the film), the transition to a slip stage is signaled by structural transformation of the interior layers in the film (which continues to maintain a rather distinct layered structure) into a dynamical phase with the intralayer order in these layers characterized by regions of a highly dislocated two-dimensional (2D) defective solid coexisting with 2D ordered (close packed) islands (these islands appear to nucleate ordering of the layers [7] when a subsequent stick-stage develops). The latter dynamical phase appears to be distinct from the less ordered ("fluidized" [56]) phase which we find during the superkinetic regime.

The central issue which I would like to address now is whether the friction in such boundary lubricated systems can be controlled. For example, can a transition to the low-friction superkinetic regime be induced by other

means, without having to slide the system with high velocities, $v > v_c$ (i.e. > 20 m s^{-1} in our case)? To this aim, a novel method for accessing low friction states of the confined lubricant is suggested [54] by the aforementioned observations [43–45], pertaining to the nature of transitions between equilibrium layered states of the film which are initiated by small (~ 1 Å) variation in the gap width. In this method dynamically controlled coupling is established between the molecular and flow degrees of freedom of the sheared lubricant and an externally driven mechanically driven mode. Here this mode takes the form of directional small-amplitude oscillatory variations of the gap width.

Results of such simulations [54] are shown in Fig. 9, confirming our expectations. In particular, small amplitude (1.5 Å) periodic variations (triangular drive with a velocity $v_{\text{osc}} = 15$ m s^{-1}) of the gap width for the 4-layer film, result (for a sliding velocity $v_s = 1$ m s^{-1}) in a most significant reduction of the frictional resistance and obliteration of the stick-slip dynamics, that is, transition to a superkinetic regime [compare Fig. 9(a,b) to the corresponding oscillation-free case shown for $v_s = 1$ m s^{-1} in Fig. 8(a,b)]. This transition is accompanied by a precipitous decrease in n_c and the normal component of the internal stress on the boundaries, σ_{int}^{zz}. On the other hand, under directional oscillations at a lower frequency ($v_{\text{osc}} = 1.5$ m s^{-1}) a somewhat frustrated form of stick-slip dynamics is maintained [compare with Fig. 9(a,b)], while oscillations at an even lower frequency ($v_{\text{osc}} = 0.3$ m s^{-1}) result in intermittent stick-slip [characterized by pronounced high static friction peaks, Fig. 9(b)] and superkinetic sliding, accompanied by large variations in n_c and σ_{int}^{zz} (with low values during the superkinetic intervals).

To understand and optimize the frequency dependence of the applied mechanical directional oscillatory coupling to the molecular shear flow motion, we suggest that the dominant operative relaxation time is that pertaining to molecular flow in-and-out of the confined zone, τ_f; other relaxation processes, such as layering of the film, intralayer ordering and the time for restoration of stick-slip dynamics subsequent to interruption of the directional oscillatory variation of the gap width while in the steady-sliding state, are related to τ_f. To estimate τ_f we have cut the pulling spring during sliding in the superkinetic regime under constant load (see $v_s = 20$ m s^{-1} in Fig. 8) and recorded the time evolutions of $n_c(t)$ (see inset in Fig. 8). Fitting the increase in the number of confined molecules by an exponential form yields $\tau_f^{N_L=4} \sim 300$ ps. We now may estimate the Deborah numbers $D_e = \tau_f / \tau_{\text{osc}}$ with $\tau_{\text{osc}} = 6 \times 10^{-10}$ m v_{osc}, yielding for $v_{\text{osc}} = 15$ m s^{-1}, $D_e = 7.5$; that is, in this regime the system is driven out of dynamic equilibrium conditions, resulting in reduced frictional

resistance (superkinetic regime), as observed in the simulations [Fig. 9(a,b) for $v_{\text{osc}} = 15$ m s^{-1}]. On the other hand, for $v_{\text{osc}} = 1.5$ m s^{-1}, $D_e = 0.75$ and a somewhat "mixed" stick-slip dynamics occurs reflecting the ability of the confined molecular system to only partially relax and explore its intrinsic dynamical states at any value of the externally applied gap variations, while for $v_{\text{osc}} = 0.3$ m s^{-1}, $D_e = 0.15$ resulting in intermittent well-defined stick-slip and superkinetic sliding intervals [57]. In fact, in the latter two cases other molecular relaxations and drive characteristic times (such as the one associated with the sliding spring-driven motion) may become operative and they, together with τ_f, should be considered in estimating the effective D_e.

The above GCMD simulations proposed and demonstrated a novel method for controlling the shear dynamics and friction in thin-film boundary lubrication [54]. The applied small-amplitude directional oscillations frustrate ordering in the film, maintaining it in a nonequilibrium dynamic state, and their effect can be controlled through selection of the oscillation period τ_{osc}, with the control parameter being $D_e = \tau_f / \tau_{\text{osc}}$, where τ_f is a characteristic time for molecular relaxation flow in-and-out the oscillating confined junction, though other characteristic structural relaxations may also be operative under other circumstances. Experimental observations pertaining to control of friction through directional coupling have been most recently made [58].

4. CONCLUSION

As has happened in many of my lectures, as well as in this one, I have run out of time (and space). Consequently I will end here by only listing some of the topics which I have originally planned to tell you about:

(i) Nano-elastohydrodynamics: structure, dynamics and flow in nonuniform lubricated junctions [23, 53].

(ii) Rate and state modeling of sliding in lubricated nanojunctions [59], with a particular application [54] to friction control via out-of-plane small amplitude oscillations (see Section 3).

(iii) More on self-selection of size and shape in nanowires [41, 42] and in zero-dimensional systems [36] (clusters) and two-dimensional thin films.

(iv) Magnetoresistance, thermopower and shot noise in nanowires [60, 61].

Research Scientific Supercomputing Center, Berkeley, CA and the Georgia Tech Center for Computational Materials Science.

REFERENCES

1. Bhushan, B., Israelachvili, J.N. and Landman, U., *Nature*, **374**, 1995, 607.

2. *Fundamentals of Friction: Macroscopic and Microscopic Processes* (Edited by I.L. Singer and H.M. Pollock). Kluwer, Dordrecht, 1992.

3. *Micro/Nanotribology and its Applications* (Edited by B. Bhushan). Kluwer, Dordrecht, 1997.

4. *Physics of Sliding Friction* (Edited by B.N.J. Persson and E. Tosatti). Kluwer, Dordrecht, 1996.

5. *Handbook of Micro/Nano Tribology* (Edited by B. Bhushan). CRC Press, Boca Raton, Florida, 1995.

6. Israelachvili, J.N., *Intermolecular and Surface Forces*, 2nd Ed. Academic Press, London, 1992.

7. Persson, B.N.J., *Sliding Friction*. Springer, Berlin, 1998.

8. See articles in Langmuir, **12**, 1996, 4481–4609.

9. Krim, J., *Scientific Am.*, **275**, 1996, 48.

10. Datta, S., *Electronic Transport in Mesoscopic Systems*. Cambridge Univ. Press, New York, 1995.

11. Imry, Y., *Introduction to Mesoscopic Physics*. Oxford Univ. Press, Oxford, 1997.

12. *Nanowires* (Edited by P.A. Serena and N. Garcia). Kluwer, Dordrecht, 1997.

13. Amontons, G., *Mémoires de l'Académie Royal A*, 1699, 257.

14. Dowson, D., *History of Tribology*. Longman, New York, 1979.

15. See review by Carpick, R.W. and Salmeron, M., *Chem. Rev.*, **97**, 1997, 1163.

16. Bowden, F.P. and Tabor, D., *Friction: An Introduction to Tribology*. Anchor Press/Doubleday, Garden City, N.Y., 1973.

17. Bowden, F.P. and Tabor, D., *Proc. Roy. Soc. A.*, **169**, 1939, 391.

18. Herzt, H., Reine, J., *Angew. Math.*, **1882**, 92, 156; also in Miscellaneous Papers, Macmillan: London, **1896**, 146; see review by Johnson, K.L., *Proc. Instrum. Mech. Eng.*, **1982**, 196, 363.

19. See review by Greenwood, J.A., in [2], p. 37.

20. Maxwell, J.C., *A Treatise on Electricity and Magnetism*. Oxford, Clarendon, 1904.

21. Sharvin, Yu.V., *Zh. Eksp. Teor. Fiz.*, **48**, 1965, 984 (*Sov. Phys. JETP*, **21**, 1965, 655).

22. Landman, U., Luedtke, W.D., Burnham, N. and Colton, R.J., *Science*, **248**, 1990, 454.

23. See Landman, U., Luedtke, W.D. and Gao, J., in [8], p. 4514.

24. See Landman, U., Luedtke, W.D. and Barnett, R.N., in [12], p. 109.

25. Landman, U., Luedtke, W.D., Salisbury, B.E. and Whetten, R.L., *Phys. Rev. Lett.*, **77**, 1996, 1362.

26. Garcia-Martin, A., Torres, J.A. and Saenz, J.J., *Phys. Rev.*, **B54**, 1996, 13448.

27. Landauer, R., *Philos. Mag.*, **21**, 1970, 863.

28. See reviews in [12].

29. Brandbyge, M., Sørensen, M.R. and Jacobsen, K.W., *Phys. Rev.*, **B56**, 1997, 14956.

30. Rubio, G., Agrait, N. and Vieira, S., *Phys. Rev. Lett.*, **76**, 1996, 2302.

31. Stalder, A. and Durig, U., *Appl. Phys. Lett.*, **68**, 1996, 637.

32. Landman, U., Luedtke, W.D. and Ringer, E.M., *Wear*, **153**, 1992, 3; see also Landman, U., Luedtke, W.D. and Ringer, E.M., in [2], p. 463.

33. Sørensen, M.R., Jacobsen, K.W. and Stoltze, P., *Phys. Rev.*, **B53**, 1996, 2101.

34. Barnett, R.N. and Landman, U., *Nature*, **387**, 1997, 788.

35. de Heer, W.A., *Rev. Mod. Phys.*, **65**, 1993, 611.

36. Yannouleas, C. and Landman, U., in *Large Clusters of Atoms and Molecules* (Edited by T.P. Martin), p.131. Kluwer, Dordrecht, 1996.

37. See articles in *Clusters of Atoms and Molecules* (Edited by H. Haberland). Springer Series in Chemical Physics 52 and 57, Springer, Berlin, 1994.

38. Bogachek, E.N., Zagoskin, A.M. and Kulik, I.O., *Fiz. Nizk. Temp.*, **16**, 1990, 1404 [*Sov. J. Low Temp. Phys.*, **16**, 1990, 796].

39. Krans, J.M., van Ruitenbeek, J.M., Fisun, V.V., Yanson, I.K. and de Jongh, L.J., *Nature*, **375**, 1995, 767.

40. Thouless, D.J. and Kirkpatrick, S., *J. Phys.*, **C14**, 1981, 235.

41. Yannouleas, C. and Landman, U., *J. Phys. Chem.*, **B101**, 1997, 5780.

42. Yannouleas, C., Bogachek, E.N. and Landman, U., *Phys. Rev.*, **B57**, 1998, 4872.

43. Gao, J., Luedtke, W.D. and Landman, U., *Phys. Rev. Lett.*, **79**, 1997, 705.

44. Gao, J., Luedtke, W.D. and Landman, U., *J. Phys. Chem.*, **B101**, 1997, 4013.

45. Gao, J., Luedtke, W.D. and Landman, U., *J. Chem. Phys.*, **B106**, 1997, 4309.

46. Van Alster, J. and Granick, S., *Phys. Rev. Lett.*, **61**, 1988, 2570.

47. Granick, S., *Science*, **253**, 1991, 1374.

48. (a) Klein, J. and Kumacheva, E., *Science*, **269**, 1995, 816; (b) Kumacheva, E. and Klein, J., *J. Chem. Phys.*, **108**, 1998, 7010.

49. Chan, D.Y.C. and Horn, R.G., *J. Chem. Phys.*, **83**, 1985, 5311.

50. Israelachvili, J.N., *J. Colloid Interface Sci.*, **110**, 1986, 263.

51. Reiter, G., Demirel, A.L. and Granick, S., *Science*, **263**, 1991, 1741.

52. Berman, A.D., Ducker, W.A. and Israelachvili, J.N., in [4], p. 51; Yoshizawa, H., Chen, Y.-L. and Israelachvili, J.N., *Wear*, **168**, 1993, 161.

53. Gao, J., Luedtke, W.D. and Landman, U., *Science*, **270**, 1995, 605.

54. Gao, J., Luedtke, W.D. and Landman, U., *J. Phys. Chem.*, **B102**, 1998.

55. The Deborah number was introduced by M. Reiner (*Physics Today*, 1964 (January), 62) as the relation between the relaxation time (τ_R) and the time scale

of the experiment $D = \tau_R/\tau_{\exp}$. He termed this number after a passage in the victory song of the prophetess Deborah — "the mountains flow before the Lord" (Judges V, 5), which is interpreted as expressing the fact that objects which seemingly remain unchanged during the human life span, may undergo significant changes when measured on a geological time scale.

56. Thompson, P.A. and Robbins, M.O., *Science*, **250**, 1990, 792.

57. Note, that it is the ratio between the molecular relaxation time and the characteristic drive-time which enter our considerations, rather than the absolute values of these quantities. Consequently, for other lubricants (with more complex molecular structures), characterized by longer relaxation times (e.g. *n*-hexadecane), significantly lower drive frequencies are required to achieve the friction-control effected demonstrated here (Gao, J., Luedtke, W.D. and Landman, U., unpublished). Additionally, when the molecular flow characteristic time, τ_f, is the dominant operative relaxation time, as is the case here, simulations for larger confinements (that is, larger confining surfaces, associated with larger values of τ_f) also require lower drive frequencies. Similar considerations apply to the friction-spring force-constant and pulling velocities.

58. Heuberger, M., Drummond, C. and Israelachvili, J.N., *J. Phys. Chem.*, **B102**, 1998.

59. Carlson, J.M. and Batista, A.A., *Phys. Rev.*, **E53**, 1996, 4153.

60. Scherbakov, A.G., Bogachek, E.N. and Landman, U., *Phys. Rev.*, **B57**, 1998, 6654.

61. See Bogachek, E.N., Scherbakov, A.G. and Landman, U., in [12], p. 35.